OXFORD UNIVERSITY PRESS Cerebral Cortex

A MODEL FOR SELF-ORGANIZATION OF VISUAL CORTEX RESPONSE MAPS AND PATCHY CONNECTIONS THAT DOES NOT REQUIRE PRESCRIBED FEATURE CATEGORIES.

Journal:	*Cerebral Cortex*
Manuscript ID:	Draft
Manuscript Type:	Original Articles
Date Submitted by the Author:	n/a
Complete List of Authors:	Wright, James; University of Auckland, Psychological Medicine Bourke, Paul; University of Western Australia, iVEC@UWA
Keywords:	spatio-temporal energy, superficial patch system, synaptic metabolic competition, synchronous oscillation, visual organization

SCHOLARONE™ Manuscripts

For Review

A MODEL FOR SELF-ORGANIZATION OF VISUAL CORTEX RESPONSE MAPS AND PATCHY CONNECTIONS THAT DOES NOT REQUIRE PRESCRIBED FEATURE CATEGORIES.

J.J. Wright,
Department of Psychological Medicine,
Faculty of Medicine,
and Liggins Institute,
University of Auckland,
Auckland,
New Zealand.
Telephone +64 9 4835 024
Fax +64 9 4820 927
Email james.wright@auckland.ac.nz
(Please use email jj.w@xtra.co.nz for correspondence during the assessment process)

P.D. Bourke,
Interactive Virtual Environment Center (iVEC)
University of Western Australia,
Perth,
Australia.

Running Title: Self-organization without feature categories.

For Peer Review

Abstract

A new model is contrasted with standard models of V1 organization. The new model proposes that synchronous oscillation and metabolic competition organize the configuration of the superficial patch system, and includes an earlier concept – that neurons form local connections within macrocolumns in a closed meshwork analogous to a Möbius strip. The new model accounts for the organization of response maps and patchy connections, including their tendency toward hexagonal rotational periodicity and the absence of patchy connections about orientation preference singularities, and explains interspecies variation in their orderliness.

Simulations of signal transmission provide a critical test of the new model. The simulations reproduce experimentally observed effects upon V1 neuron responses to visual lines, as a function of the line's orientation, direction of movement, speed, and length. Neither selective feature-specific response of neurons (as in standard models, which are unable to explain the same data) nor selective neuron responses to particular spatial and temporal frequencies of inputs are assumed.

Further anatomical and physiological tests for the new model are proposed, and the implications for information flow in the cortex are briefly considered.

Key words · spatio-temporal energy · superficial patch system · synaptic metabolic competition · synchronous oscillation · visual organization

Introduction

In this paper we derive a model for self-organization of the cortical superficial patch system and link this to earlier work (Wright et al 2006; Wright & Bourke 2008) in which we proposed that synaptic connections within a macrocolumn form a closed, recurrent, network analogous to the surface of a Möbius strip. The combined model contrasts with standard models of cortical organization and is able to explain otherwise unresolved issues in contemporary visual and cortical physiology.

Unresolved issues.

Since the discovery that individual cells in the primary visual cortex (V1) respond with an Orientation

For Peer Review

Preference (OP) to visual lines of differing orientation (Hubel and Wiesel 1959), attempts to analyze the response organization and explain its relationship to cortical function (von der Malsberg 1973; Willshaw and von der Malsberg 1976; Swindale 1996) have played a pivotal role in neuroscience. The surface organization of OP in V1 has recently been compared with appropriate random surrogates, and shown, in some species, to approximate an hexagonal rotational periodicity, in which each roughly delineated macrocolumnar unit exhibits all values of OP arrayed around a pinwheel (Paik and Ringarch 2011; Muir et al 2011). Varying chirality and orientation of the pinwheels achieves continuity of OP at the columnar margins, thus producing linear zones and saddles. In any individual irregular variation from the average periodicity is seen, and some species exhibit little or no sign of this ordering. Because of this marked interspecies variation, serious doubt has been expressed that the pattern is of functional significance at all, since response maps are absent in some species without those species having any apparent deficit in vision (Horton and Adams 2005).

A further puzzle of V1 organization is posed by the superficial patch system. This system, composed of relatively long-range, largely excitatory (McGuire et al 1991, Hirsch and Gilbert 1991) patchy connections (Gilbert and Wiesel 1979; Rockland and Lund 1983) is ubiquitous in cortex (Muir and Douglas 2011) and has a functional relationship to OP. Patchy connections develop before sensory afferents reach the cortex (Price 1986; Callaway and Katz 1990; Durack and Katz 1996; Ruthazer and Stryker 1996) and do not arise or terminate in the vicinity of OP singularities. Instead, near singularities, connections are apparently diffuse and local (Sharma et al 1995; Yousef et al 2001;Mariño et al 2005; Muir and Douglas 2011; Buzás et al 2006). Yet patchy connections link areas of common OP ("like-to-like") over distances several times the diameter of a macrocolumn (Mitchison and Crick 1982; Gilbert and Wiesel 1989; Buzás et al 2006; Muir et al 2011), are periodic on roughly the same interval as OP, and are largely patch-reciprocal (Rockland and Lund 1983; Angelucci et al 2002). It has been shown that formation of patchy connections must depend on the supply of information from the field by presently unknown means, rather than being explicable from considerations of neural growth *per se* (Muir and Douglas 2011). Muir and Douglas's analysis emphasizes the absence of patchy connections in the vicinity of singularities as a crucial aspect requiring explanation in future models.

Initial belief that response to simple oriented lines in the visual field formed the basis of OP maps has been undermined in two ways. Firstly, maps of OP appear in the cortex prior to visual experience (Wiesel and Hubel 1974; Blakemore and Van Sluyters 1975; Sherk and Stryker 1976) - although it is argued that structured stimuli may arise from retinal inputs in the absence of visual experience (Albert et al 2008; Ringarch 2007; Paik and Ringach 2011). Secondly, and more recently, Basole and

For Peer Review

colleagues, who tested OP using stimulus lines moving at different speeds, and oriented at differing angles to the line of movement of the stimulus, found OP to be a function of these variables to such a degree that for lines oriented non-orthogonally to the direction of movement, OP could vary progressively with increments of speed to an asymptotic limit of 90 degrees (Basole et al 2003, 2006). They also found that this effect was attenuated for lines of progressively greater length. They, and subsequent workers, were able to explain their results by considering the temporal and spatial frequencies associated with the moving stimuli (Baker and Issa 2005; Mante and Carandini 2005; Basole et al 2006) and concluded that the primal stimulus characteristics are not isolated features such as orientation, direction and speed, but a reflection of the "spatio-temporal energy" (that is, the spatial and temporal Fourier components) of the moving visual stimulus' projection to V1. Their results correspond to earlier single unit results in which tuning of V1 neurons to spatial and temporal frequency (DeAngelis et al 1993) was demonstrated. In this interpretation classical OP is the low stimulus-velocity limit of frequency selectivity of neuronal response. But it is not known how the spatial and temporal characteristics of a moving stimulus become transformed into determinates of individual cell firing. The findings also raise the possibility that the choice of stimulus type determines the kind of feature-detection that V1 neurons will exhibit.

In further respects OP properties have proved more complicated than simple initial expectation. Estimates of OP near singularities show the measure, in response to drifting gratings, to be highly adaptively interactive with prior, contextual, stimuli– yet in linear zones, the measure is stable (Dragoi et al 2001). Also, the activation of neurons with a particular OP generates travelling electrocortical waves surrounding the site of stimulation (Benucci et al 2007) and these waves do not appear to be limited to propagation along "like to like" couplings.

Standard models and their problems

Explanation of organization of OP has been attempted in a group of now-classical theories, which we will refer to as "standard models", following the comparative description of models introduced by Swindale (Swindale 1996). Dimension reduction methods (Kohonen 1982; Dubin and Willshaw 1987; Durbin and Mitchison 1990) show that the response maps of OP, eye preference (OC), direction preference (DP) and spatial-frequency preference (SF) are consequences of requiring continuity and completeness of representation of the full range of each response property, in a two-dimensional representation in which every type of response property occurs within any small area on the surface of V1 (Swindale 1996; Carriera-Perpiñán et al 2005). The same ordering is also explained as a consequence of competitive Hebbian learning among small neighborhood assemblies of excitatory

For Peer Review

neurons, driven by spatially filtered cortical noise (Grossberg and Olson 1994). Separate spatial filters each distinguish a prescribed type of response, and total synaptic gain is conserved during the training, so that at each point in the field

$$\sum_{k=1}^{n} f_k(x_k) = K \qquad (1)$$

where x_k is a measure of a response property, $f_k(x_k)$ is an increasing function of x_k, and K is the maximum local synaptic weight. Of the types of response, the response to oriented lines is the cardinal feature, and the other categories follow from filtering on the input pathway (OC, DP) or as a secondary corollary of OP organization (SF).

All standard models depend on seeding with oriented lines, in one way or another (von der Malsberg 1973; Durbin and Mitchison 1990; Obermayer et al 1990, 1992; Tanaka 1990; Swindale 1982,1992; Miyashita and Tanaka 1992 ; Grossberg and Olson 1994) and related models avoiding this limitation do not accurately reproduce response maps (Linsker 1986a,b,c; Miller 1994). More recent models dependent on retinal input (Albert et al 2008; Ringarch 2007; Paik and Ringach 2011) still ascribe response to oriented lines a primary role in the emergent functional architecture.

Inhibition at greater range in the cortex than the range of excitatory connections is also necessary to produce Hebbian maps of OP in standard models. The findings of Basole and colleagues (Basole et al 2003) pose a particular challenge to the standard models, since the inhibitory surround's role is to suppress the connections responding to stimulus lines which are orthogonally oriented, and facilitate excitatory connections along the line of OP. Furthermore, anatomical evidence for long-range inhibitory connections is lacking (Swindale 1996) and aligned excitatory connections within macrocolumns are not apparent. More complex patterns of interconnection, in the form of interwoven meshes, have been recently demonstrated (Perin et al 2011) and are considered later in this paper.

Synchronous oscillation, synaptic self-organization, metabolic competition and maximization of network information storage

In our earlier work (Wright et al 2006; Wright & Bourke 2008) we hypothesized that synchronous oscillation may provide a mechanism for the coordination of synaptic consolidation and thus form OP maps, although we disregarded patchy connections. The extended model to be presented here relies on the same hypothesis.

For Peer Review

Synchronous oscillation of pulses and local field potentials is a ubiquitous aspect of cortical activity (Eckhorn et al 1988, 1990; Bressler et al 1993; Gray et al 1989; Singer 1999; Cohen and Kohn 2011) and has been proposed as a solution to the "binding problem" of perceptual grouping and cognitive processing (Eckhorn 1990; Carpenter et al 1991; Singer 1999). Synchrony is a broad-band phenomenon in the temporal frequency domain, and oscillation in the gamma range produced by local excitatory-inhibitory cyclic firing is a principle cortical source of oscillation (Freeman 1991; Hausenstaub et al 2005) so that "synchronous oscillation" is often most apparent in the gamma band. Three neural mechanisms have been advanced to explain synchrony. Firstly, driving of neurons by synchronous signals from the thalamus (Steriade 2000), which is applicable to the initiation of feature binding (eg Singer 1999). Secondly, local inter-inhibitory oscillation (Schillen and Konig 1994; Traub et al 1996; Whittington et al 2000), a theory developed to explain oscillations in the hippocampus but possibly a more widely contributory mechanism to the local generation of oscillation. Thirdly, rejection of out-of-phase pulses during dendritic summation (Robinson et al 1998; Wright et al 2000, 2009, 2010; Chapman et al 2002). The third mechanism is of most importance in the present context, as it describes an average property of activated cortex, and thus may provide the broad organization of the cortical field required to co-ordinate synaptic development. This type of synchrony and synchronous oscillation appears in simulations that also accurately reproduce spectra, cross-correlations and excitatory/inhibitory timings characteristic of activated cortex (Wright 2009). It is a consequence of wave interactions, and is at a maximum when equilibrium in the exchange of signals between all excitatory and inhibitory neurons is approached (Wright 2010). It is convenient to distinguish the contributions of short-range and longer-range axonal connections, and their associated synaptic weights and pulse coincidence rates, to the synchronous field. Then, at any position $\mathbf{q}$, the magnitude of zero-lag oscillation of dendritic potentials is given as $J^{\mathbf{q}}$, and the total synchronous field at equilibrium is

$$\sum_{\mathbf{q}} J^{\mathbf{q}} = \sum_{\mathbf{q}} \left(\sum_{\mathbf{R}} \alpha_{\mathbf{R}}^{\mathbf{q}} C_{\mathbf{R}}^{\mathbf{q}} + \sum_{\mathbf{r}} \beta_{\mathbf{r}}^{\mathbf{q}} C_{\mathbf{r}}^{\mathbf{q}} \right) \rightarrow \max \qquad (2)$$

where $\mathbf{r}$ and $\mathbf{R}$ are vector positions distant from $\mathbf{q}$, measured along short-range and longer-range connections respectively, $\alpha_{\mathbf{R}}^{\mathbf{q}}, \beta_{\mathbf{r}}^{\mathbf{q}}$ are synaptic gains of synapses linking $\mathbf{q}$ and $\mathbf{r}, \mathbf{R}$, and $C_{\mathbf{R}}^{\mathbf{q}}$ and $C_{\mathbf{r}}^{\mathbf{q}}$ are aggregate pre-/post-synaptic pulse coincidence rates between neurons at $\mathbf{q}$ and $\mathbf{r}, \mathbf{R}$. These terms can be introduced to a normalized learning rule, as follows.

Physiological findings indicate that the Hebb rule operates under the concurrent influence of pre-

For Peer Review

synaptic cooperation of synapses (Tsukada and Fukushima 2010) and synaptic competition for vital metabolic resources – notably neurotropins (Harris et al 1997; van Ooyen and Willshaw 1999; van Ooyen 2001; Elliot and Shadbolt 2002) but probably for many factors. The pre-synaptic cooperative effects imply the synchronous field must facilitate Hebbian consolidation, while metabolic resource competition imposes a form of competitive normalization. Steady-state solutions of the mass action effects operating upon the many synapses at a point in the neural continuum can then be expressed in sigmoid functions

$$\alpha_{\mathbf{R}}^{\mathbf{q}} = 2(1+\exp[-(hC_{\mathbf{R}}^{\mathbf{q}} + gJ^{\mathbf{q}})])^{-1} \quad (3a)$$

$$\beta_{\mathbf{r}}^{\mathbf{q}} = 2(1+\exp[-(hC_{\mathbf{r}}^{\mathbf{q}} + gJ^{\mathbf{q}})])^{-1} \quad (3b)$$

$hC_{\mathbf{r},\mathbf{R}}^{\mathbf{q}}$ describes the Hebbian effect, $gJ_{\mathbf{r},\mathbf{R}}^{\mathbf{q}}$ describes the pre-synaptic cooperative effect, and h,g represent some ascending functions of $C_{\mathbf{r},\mathbf{R}}^{\mathbf{q}}$, with the consequent property that if $h \wedge g$ are positive valued, then at equilibrium $\alpha_{\mathbf{R}}^{\mathbf{q}} \wedge \beta_{\mathbf{r}}^{\mathbf{q}}$ tend to a value of two, and if $h \wedge g$ are negative valued, then at equilibrium $\alpha_{\mathbf{R}}^{\mathbf{q}} \wedge \beta_{\mathbf{r}}^{\mathbf{q}}$ tend to a value of zero. Thus the signs of $h \wedge g$ enable simple representation of success or failure in a "winner take all" metabolic competition.

We further assume that evolutionary pressure would develop neural networks of maximum information processing capacity. Sparseness of synaptic connections, their noisiness and weakness, and the wide variation of synaptic weights, is consistent with the maximization of information storage per unit volume of cortex (Varshney et al 2006). The most simplified case consistent with experimental findings (O'Connor et al 2005a,b) is where there are only two distinct synaptic states - saturated gain and zero gain. In that case, in equations (3a,b) $\alpha_{\mathbf{R}}^{\mathbf{q}}, \beta_{\mathbf{r}}^{\mathbf{q}}$ have maximum/minimum values 2 or 0, with synapses able to alternate between the two states, depending on available resource. Where metabolic resources can sustain only half the synapses in the saturated state, then H, the Shannon entropy for n synapses, based on unconditional probabilities, is maximized

$$H = -\sum_{i=1}^{n} p_i \log_2 p_i \rightarrow \max \quad (4)$$

$p_i = 0.5$ for each synapse - and the average synaptic gain is unity.

Descriptions of Models

For Peer Review

We next present a set of three models of response properties, in a related formalism. Firstly, a representation of the connection structure which emerges in standard models. Secondly, a model depending on synchrony and metabolic competition – differing from the assumptions of the standard model – that accounts for the emergence of patchy connections. Finally, a reconciliation of the second model with our earlier concept of local Möbius connectivity, providing a new, more complete model and enabling critical test against the standard models.

Standard model

The emergent connection structures of standard models for OP, where OP is measured using slowly moving stimuli (Swindale 1996), implicitly including representation of OC, DP and SF, can be represented in a form permitting comparison with the two subsequent models, as follows:

Figure 1 shows an idealized set of adjacent macrocolumns in V1, arranged in an hexagonal array of elements, each containing typical OP singularities, linear zones and saddles. Superimposed, as semi-transparent tubes, are hypothetical lines of excitatory connections linking excitatory neurons together so they respond selectively to oriented visual stimuli transmitted to the classic receptive fields (cRF). "Like to like" connections bridge areas of common OP between macrocolumns, in the fashion of patchy connections.

[Figure 1 about here]

Positions in the field can be defined as:

$\{\mathbf{R}\}$ (the global field). Vector positions on the surface of V1.

$\{\mathbf{r}\}$ (the local field). Vector positions within a column, of diameter a little less than the spread of dendritic and local intracortical axonal trees of pyramidal cells in V1 and embedded in $\{\mathbf{R}\}$.

$\{\mathbf{R}\} \equiv \{\{\mathbf{r}\}_i\}$ A set of similar reference frames to $\{\mathbf{r}\}$ such that V1 is tiled by the set.

For Peer Review

Interactions between $\{\mathbf{R}\}$ and $\{\mathbf{r}\}$ are representative of all interactions between the global field and each $\{\mathbf{r}\}_i$. "Like to like" connections act as a mapping from the global (V1) to the local (macrocolumnar) field. The two-fold rotational symmetry of oriented lines results in the representation at the singularity of stimulus line angles from $0-\pi$, over $0-2\pi$. Consequently the "global to local map" (Alexander et al 2004) can be represented as a 2:1 complex-multiplication map

$$\mathbf{R} \Leftrightarrow \mathbf{r}^2(\vartheta \pm \varphi) \tag{5a}$$

where the bracketed terms $(\vartheta \pm \varphi)$ indicate that only a subset of $\{\mathbf{R}\}$ and $\{\mathbf{r}\}$ - those points with common OP, ϑ, within some angular deviation, φ - are connected by excitatory connections. Also, excitatory connections between any two points, 1 and 2, within each macrocolumn link points of common OP

$$\mathbf{r}_1(\vartheta \pm \varphi) \Leftrightarrow \mathbf{r}_2(\vartheta \pm \varphi) \tag{5b}$$

With appropriate orientation and chiralities, $\{\{\mathbf{r}\}_\mathbf{i}\}$ maintain continuity and completeness at the borders, with resulting linear zones and saddles.

A Euclidian model of the superficial patch system

The purpose of this model is to explain the origin of the superficial patch system as a consequence of supply of information from the neural field, as inferred by Muir and Douglas (Muir and Douglas 2011) and also to explain the continuity of OP maps, their tendency to hexagonality and their lack of order in some species. We call this model "Euclidean" because the pattern of synaptic connections it predicts can be simply represented on the Euclidean plane, as in most neural field models (eg Wilson and Cowan 1973; Freeman 1975; Haken 1976; Nunez 1981; van Rotterdam et al 1982; Jirsa and Haken 1996; Robinson et al 1997; Rennie et al 2000; Robinson et al 2001; Chapman et al 2002; Wright et al 2003; Wright 2010).

Embryological observations (Price 1986; Callaway and Katz 1990; Durack and Katz 1996; Ruthazer and Stryker 1996) indicate the developing cortex extends lateral synaptic connections at two scales, corresponding to intracortical short-range and to long-range connections spanning more than a macrocolumn, each with densities of potential synaptic contact to surrounding neurons declining

For Peer Review

exponentially with range, and with the two types of connections arising from partially or wholly distinct neuron populations. Emergence of a similar organization, leading to a small world configuration, is seen in neural cultures (Downes et al 2012). We will not attempt to explain why connections on two scales occur. The selection of consolidated connections from the uniform initial state, to create characteristic patchy connections, is to be explained, as is the high degree of variation of these patches in different species.

Our hypothesis is that pre-natal development proceeds under cell pruning and metabolic competition until a distribution of saturated synapses emerges, such as to sustain the average state of the activated, synchronously oscillating, cortex in equilibrium, and thus, reciprocally, to sustain the synapses in stable states. That is, we find the conditions in which the maximization of equation (2) is realized via equations (3a,b, 4) and equations (6a,b), which are next defined.

Pre-/post-synaptic pulse coincidence rates ($C^{\mathbf{q}}_{\mathbf{R}}$ and $C^{\mathbf{q}}_{\mathbf{r}}$) generated via intracortical and long-range connections at any point, $\mathbf{q}$ in the field, are required in equation (2), and can be parameterized from neural field theory, summarized in the Appendix:

$$C^{\mathbf{q}}_{\mathbf{R}} = r\frac{N_\alpha}{N}\frac{1}{\lambda_\alpha}\exp[-\lambda_\alpha|\mathbf{q}-\mathbf{R}|]\overline{Q}^2 \qquad (6a)$$

$$C^{\mathbf{q}}_{\mathbf{r}} = r\frac{N_\beta}{N}\frac{1}{\lambda_\beta}\exp[-\lambda_\beta|\mathbf{q}-\mathbf{r}|]\overline{Q}^2 \qquad (6b)$$

The fraction of coincident pre- and post-synaptic pulses that coincide is $r \in \{0-1\}$, a declining function of $|\mathbf{q}-\mathbf{r},\mathbf{R}|$ and $\overline{Q}$ is the mean field excitatory pulse rate. N_β and N_α are numbers of intracortical and long-range pre-synapses per neuron; λ_α and λ_β are inverse length constants for the initial distribution of pre-synapses on the longer-range and shorter-range axonal trees respectively, and $N_\alpha + N_\beta = N$.

Emergence of patchy connections in hexagonal array, with spared zones about singularities

The anatomical findings of Boucsein and colleagues (Boucsein et al 2011) indicate that $N_\beta \geq N_\alpha$ and $\lambda_\alpha < \lambda_\beta$. In principle, via equations (6a,b), equation (2) has parameter ranges which may vary from $N_\beta >>> N_\alpha$ to $N_\beta <<< N_\alpha$, and from $\lambda_\alpha <<< \lambda_\beta$ to $\lambda_\alpha \approx \lambda_\beta$.

For Peer Review

We first consider the case $N_\beta >>> N_\alpha$ and $\lambda_\alpha <<< \lambda_\beta$, where long-range connections are sparse, but long-range, compared to short-range connections, and show that this leads to an orderly solution. We avoid difficult analytic and numerical methods to maximize equation (2) by appeal to arithmetical, physical, and geometric requirements for the solution.

Since $N_\beta >>> N_\alpha$, the terms $\sum_{\mathbf{r}} \beta_{\mathbf{r}}^{\mathbf{q}} C_{\mathbf{r}}^{\mathbf{q}}$ $(\beta_{\mathbf{r}}^{\mathbf{q}} = 2)$ in equation (2) are the major terms, and are largest, according to equation (6b), if the cell bodies of origin of short-range saturated synapses are clustered together, excluding long-range saturated connections, so as to minimize distances of separation, $\{|\mathbf{q}-\mathbf{r}|\}$, while also maximizing the number of such connections by forming the largest possible aggregates connected wholly by short-range connections. Such an aggregate we term a $\mathfrak{A}$-patch.

Neural field simulations indicate (Wright 2009, 2010) that maximization of mean value of pre-/post-synaptic coincidence, r, in equations (6a,b) requires reciprocal saturated connections, and without long-range couplings, in the presence of neural noise, the mean value of r tends to zero – so some long-range saturated synapses must exist. Because cell bodies in $\mathfrak{A}$- patches must be gathered at close proximity, then cell bodies connected by long-range saturated connections must form some inter-dispersed $\mathfrak{O}$ connection system, and stable configuration then requires that the α system and the β-patches have regular periodicity.

Consequently, the $\mathfrak{O}$ system must form some regular polygonal mesh, tiling the cortical surface, and embracing $\mathfrak{A}$- patches. Of the three regular polygonal tilings of the plane, that mesh permitting the embracement of the largest intervening patches, is an hexagonal tiling. From equations (6a,b), there is a critical distance, $|\mathbf{q}-\mathbf{r},\mathbf{R}| = x$, where $x = (\ln\frac{N_\beta \lambda_\alpha}{N_\alpha \lambda_\beta})/(\lambda_\beta - \lambda_\alpha)$ such that $C_{\mathbf{R}}^{\mathbf{q}} > C_{\mathbf{r}}^{\mathbf{q}}$ over distances greater than x. Therefore, saturated pre-synapses on axons from cell bodies in the α system must preferentially form at ranges $> x$, to have competitive metabolic advantage over short-range synapses from other cell bodies near the same position. Therefore the α system must contain α-patches. Long range connections from individual cells in the α system extending to make connections with other α-patches over several times the diameter of the β-patches would further increase the mean value of r.

For Peer Review

The outcome is that β-patches, of radius approximate to x, become enclosed in an hexagonal mesh of $\mathfrak{o}$-patches, of inter-patch distance approximate to x. (See Figure 2, Top.)

[Figure 2 about here]

Between-scale mapping and continuity in adjacent macrocolumns

Since maximization of the terms $\sum_{\mathbf{r}} \beta_{\mathbf{r}}^{\mathbf{q}} C_{\mathbf{r}}^{\mathbf{q}}$ in equation (2) requires maximum resonance, the α-patches must form recipocal saturated connections with some neurons in the β- patches such that spatial frequencies of synchronous oscillation are matched to maximum resonance throughout the field. This implies a 1:1 mapping of saturated connections between scales is created. Thus the centres of β-patches become singularities corresponding to the centre point of a map of positions radiating to and from the complete surrounding cortical surface, without the angular restrictions in equations (5a,b) – ie:

$$\mathbf{R} \Leftrightarrow \mathbf{r} \qquad (7a)$$

Within each macrocolumn, excitatory connection strengths are not functions of the angles ϑ,φ, but simply inverse functions of distance of separation

$$\mathbf{r}_1 \Leftrightarrow \mathbf{r}_2 \qquad (7b)$$

[Figure 3 about here]

Maximization of resonance is further achieved if adjacent β - patches have homologous points on their respective 1:1 maps at shortest distances. This requires adjacent local maps to be aligned with orientations and chiralities as mirror images, each of the other – a condition which can be approximated with broken symmetry, and which ensures continuity of maps at their borders. (See Figure 3).

Interspecies variation of map organization.

For Peer Review

As mentioned in the Introduction the repeating hexagonal symmetry of OP and the superficial patch system is approached as an idealization in some species, while in others it is effectively absent (Horton and Adams 2005). We showed above that at the limits $N_\alpha <<< N_\beta$ and $\lambda_\alpha <<< \lambda_\beta$ the patchy connection meshwork approaches perfect hexagonal rotational symmetry (see Figure 2 Top). At other limiting parameter ratios this is not the case.

If $\lambda_\alpha \approx \lambda_\beta$, no distinction between long-range and short-range connections is present, and an ordered structure based on range distinction could not emerge. Retaining the restriction $\lambda_\alpha <<< \lambda_\beta$, but allowing $N_\alpha \geq N_\beta$, then the size of β - patches would be diminished and regular packing of any sort need not emerge (see Figure 2 Bottom).

The absence of apparent order need not imply a loss of functionality. So long as $\lambda_\alpha < \lambda_\beta$ then connections maximizing co-resonance between any restricted area of cortex and its greater surround would still occur.

Success and failure of the Euclidean model

The Euclidean model accounts for the disposition of patchy connections, their absence about singularities, and the associated hexagonal periodicity of patchy connections. But the model fails since the $0-\pi$ range of OP about a singularity is represented twice.

A unified Euclidean and Möbius model

Assumptions made for the Euclidean model can be modified so as to overcome that model failure, by combining the concept of organization of short-range intracortical synapses into a form analogous to a Möbius strip (Wright et al 2006; Wright & Bourke 2008) with the Euclidean model's explanation of patchy connection evolution and hexagonal symmetry. This is achieved by making the assumption that competition for metabolic resources takes place at a smaller scale than necessarily implied in the Euclidean model, so that synapses arising from closely adjacent parts of the same axon must compete for metabolic resources. A site of connection, $\mathbf{q}$, can now be subdivided to two locales, $\mathbf{q}'$ and $\mathbf{q}''$, representing the terminations of saturated, versus zero-saturated, synapses from $\mathbf{r},\mathbf{R}$. Because of the close physical proximity of $\mathbf{q}'$ and $\mathbf{q}''$, the resulting 1:1 map is the projection of a Euclidean plane (the patchy system of V1) to a Möbius plane centered about each OP singularity. The topological identity of a Möbius strip and a circle permits retention of the 1:1 global-to-local maps of the

For Peer Review

Euclidean model. This geometry can be physically realized in a meshwork of excitatory synaptic connections closing after circling twice about a central point in each macrocolumn, and receiving patchy connections from opposite sides of the global field at closely situated positions, but on opposite limbs, on the mesh (see Figure 4). Because of the angle-doubling property of projection to a Möbius plane, angles of projection from the global to the local maps from $0-2\pi$ are now folded about the singularity, corresponding to the angle-doubling about OP singularities, and continuity of OP in surrounding macrocolumns is identical to that of the standard model. Adjacent points $\mathbf{q}'$ and $\mathbf{q}''$ designated as saturated or zero-saturated may be dynamically alternating on short time-scales.

In analogy to the preceding models

$$\mathbf{R} \Leftrightarrow \mathbf{r}^{[2]} \tag{8a}$$

and

$$\mathbf{r}_1^{[2]} \Leftrightarrow \mathbf{r}_2^{[2]} \tag{8b}$$

The superscript notation [2] is used to indicate the resemblance, viewed from a third dimension, between projection from a Euclidean to a Möbius plane and the complex-multiplication projection between two Euclidean planes ascribed to the standard model in equation (5a).

[Figure 4 about here]

We subsequently refer to this unification of the Euclidean model with our earlier Möbius model, as "the Möbius model".

A Critical Test – Simulation of "Spatio-temporal Energy" responses

……

Comparison of models

The standard and Möbius models can be compared in a critical test – reproduction of the findings of

For Peer Review

Basole and colleagues (Basole et al 2003). The standard model is expected to fail for the reason given in the Introduction – that the inhibitory surround on which standard models depend ought to suppress the near-orthogonal rotation of OP seen to occur at high speeds of translation of visual lines that are not orthogonally orientated to the line of passage – but this requires to be demonstrated.

According to the Möbius model, the lateral transfer of transient contextual signals over the established patchy system, to each macrocolumn, can be expressed as

$$O(\mathbf{R},t) \Rightarrow \{O(\mathbf{r}^{[2]},t+\frac{|\mathbf{R}+\mathbf{r}+\mathbf{C}_i|}{v})\}_i \qquad (9a)$$

where O is an object representation projected to V1 by the direct visual path, and relayed to representative macrocolumns, $\{\{\mathbf{r}\}_i\}$ (where each $\{\mathbf{r}\}_i$ has appropriate orientation and chirality), $\mathbf{C}_i$ is vector distance from the origin of $\{\mathbf{R}\}$ to the origin of $\{\mathbf{r}\}_i$, and v is the velocity of polysynaptic wave transmission.

The equivalent contextual signal transmission in the standard model is

$$O(\mathbf{R},t) \Rightarrow \{O(\mathbf{r}^{2}(\vartheta \pm \varphi),t+\frac{|\mathbf{R}+\mathbf{r}+\mathbf{C}_i|}{v})\}_i \qquad (9b)$$

Simulations using equations (9a) and (9b) can be compared to the experimental findings of Basole and colleagues. Successful reproduction of their findings would also explain the tuning of V1 neurons to spatial and temporal frequency reported by DeAngelis and colleagues (DeAngelis et al 1993) since the mathematical identity of these two types of findings has already been demonstrated (Baker and Issa 2005; Mante and Carandini 2005).

Method of Simulation

Equations (9a) and (9b) were each applied in a simulations of an hexagonal array of seven adjacent macrocolumns. Cortical magnification factor was not considered a significant distortion in a comparatively small cortical area. For simplicity we considered the monocular case, in the area of V1 outside the zone organized into ocular columns, although the simulation architecture is readily modified to include the binocular case, with little implication for the results to be reported. The

For Peer Review

assumed diameter for each macrocolumn was 300 microns, and wave speed for transcortical polysynaptic propagation 0.1 m/s (Bringuier et al 1999). Simulation time-step was 0.1 ms. Units of distance or length subsequently referred to, are multiples of the radius of a macrocolumn – 150 microns.

A moving line in the visual field, relayed by the direct visual pathway to the cRF of each macrocolumn was represented graphically as a red bar, moving with a speed measured as *bar speed/wave speed*. The lag-transmitted image of the red bar, relayed as subthreshold activation to each macrocolumn via the superficial patch system) was shown in green, with a 3:1 reduction from the global to local scale. Passage of the relayed visual stimulus across a macrocolumn was shown as bright illumination about the zone of subthreshold activation, to indicate that input to the cRF from the direct visual pathway and contextual signals had caused triggering of action potentials. The epoch of illumination began at the time-step at which the red bar crossed the center of each macrocolumn, and continued until the time-step at which the red bar passed beyond the macrocolumn's boundary. In a single simulation the red bar travelled across the entire hexagonal array from left to right, with constant speed, direction and orientation. The orientation of the red bar to the line of passage was measured as *bar angle* from 0 degrees, where the bar was oriented orthogonally to the direction of travel, to ± 90 degrees, where the bar was oriented in the direction of travel.

During the illuminated epoch, the average angle from the macrocolumn singularity to the centers of action potential generation (ie, all points on the green line) was calculated at each time-step, and shown as a black arrow. This indicated the part of the macrocolumn's neural field which was currently most stimulated by the combination of the cRF and the contextual input – and thus indicated the part of the macrocolumn with a response preference (*apparent OP*) for the particular bar movement. (In relation to conventional experimental measures, a change in the sector of the macrocolumn which is maximally stimulated is equivalent to an equal change in the angle of approach of the bar needed to maintain stimulation of the same sector). The black arrow angle was averaged over a window beginning after the red bar had passed the center of the macrocolumn by a distance equal to 10% of macrocolumn radius, and extending from the 10^{th} percentile to the 20^{th} percentile of that radius, thus obtaining an estimate of the apparent OP during the cRF activation time. At low bar speeds this corresponded to approximately the 100th to 200th time-step in the illuminated epoch.

The standard error (SE) of the black arrow angles was calculated from 11 equally spaced time steps through the averaging window, independently of bar speed. The SE, and the breadth of the illuminated area during the illuminated epoch, gave indications of the breadth of OP tuning, although

For Peer Review

tuning response curves were not simulated *per se*.

Combinations of bar-length, orientation of the bar to the direction of movement, and bar speed, were then systematically varied in separate simulations. Their effects on OP, measured at the central local map of the hexagonal group, were obtained as *OP difference* – a measure of the change in OP as a function of these variables - calculated as

$$OP\ difference = \frac{[apparent\ OP] - [reference\ OP]}{2} \qquad (10)$$

where *reference OP* was the apparent OP found at the lowest bar speed applied (bar speed/wave speed = 0.1), the angular difference was the smaller of the differences between the apparent and reference OP angles (to avoid wrap-around ambiguities), and division by 2 preserves the convention that OP is on the range $0 - \pi$.

The results shown in Figures 6 and 7 showed some systematic variation with choice of duration for the averaging window, but no qualitative differences. A change in estimated wave speed was also without quantitative effect, when averaging window length was appropriately adjusted, and results were interpreted as the ratio of bar-speed and wave-speed.

Simulation Results

Simulation features for the Möbius model are shown in Figure 5, as the visual stimulus of a moving bar, travelling at half the wave conduction speed, orientated at 60 degrees to the line of passage, and moving from left to right across V1, mimics activation of the macrocolumns.

[Figure 5 about here]

Figure 6 graphs OP difference versus bar speed / wave speed, for bar angles 0 to ± 90 in the Möbius model, calculated for a bar length of 4 units. The inserts show three examples of the change in apparent OP with increasing bar speed for bar angle = 45 degrees, showing the orthogonal transformation of apparent OP from the lowest to the highest bar speed, and also that the angular breadth of cortical subthreshold activation, analogous to the width of tuning of the OP response, is narrow at the lowest bar speed, and broadens as bar speed approaches wave speed.

For Peer Review

[Figure 6 about here]

For the case of bar-angle 90 degrees (a line oriented along its direction of passage) Figure 6 shows that velocity exerts no OP difference. In contrast, for the case of bar-angle zero degrees (a line oriented orthogonally to its direction of passage, as in classical measurements of OP) no OP difference is seen until, as bar speed approaches wave speed, a 90 degree change in apparent OP takes place at a single increment in speed. This corresponds to transition to a "motion streak", as object movement blurs resolution in the direction of motion. Increasing OP difference with bar speed at other bar angles is a more gradual development of the same effect – that is, mixing of responses to object speed and to object orientation.

The impact of line extension on the relations between OP, speed, and object orientation, are shown in Figure 7. Here, graphs in the form of figure 6 are shown for bar length 1, bracketed above and below by limiting cases of small (0.25 units) and very large (16 units) bar lengths.
With small bar length, OP difference diminishes for all bar speeds compared to intermediate bar lengths, and particularly so at high bar speeds. For bar speeds approaching wave speed, SEs are very high, and for bar angle zero, the apparent OP apparently undergoes sequential orthogonal shifts as bar speed increases through this critical speed range.[1] These features show the highly unstable relationship between short lines of corresponding high space frequency orthogonal to their direction of motion, and their "motion streak" spatial-temporal frequency in the direction of motion itself.

In contrast, for very large bar length, all bar angles exhibit small OP differences at increasing bar speeds, until apparent OP undergoes an orthogonal transformation at a bar speed which differs with each bar angle.

[Figure 7 about here]

These results match the findings of Basole et al 2003 in the moderate bar length and bar speed ranges, while the limiting cases confirm indirectly that apparent OP has components of response to the spatio-temporal frequencies of the visual stimulus, as was shown by fitting of Fourier components to the data

[1] The second reversal of OP difference can be shown to result from the development of dual solutions to the map equation (9a) that occurs when the visual stimulus bar has passed the system origin and bar speed is greater than wave speed.

For Peer Review

(Baker and Issa 2005; Mante and Carandini 2005; Basole et al 2006).

In contrast, simulations using the standard model showed a limited effect. The example shown in Figure 8 assumed a restriction to $\varphi = 45$ degrees, in equations (5a,b, 9a,b) – that is to a 90 degree wedge of mutually excitatory connections about the singularity for any given OP – representing generous excitatory overlap of adjacent areas of OP. To attain the full range of OP difference actually found experimentally, φ would require a value of 180 degrees, which contradicts the principle of mutual inhibition on which standard models are based.

[Figure 8 about here]

Proposed further anatomical and physiological tests

Since the Möbius model passes its first critical test, it may be asked what further tests are practicable. Detailed simulations developed from those described above would permit further precision of match to experiment. The architecture of the simulations can be extended to include binocular columns, cortical magnification factor, improved estimates of dendritic time constants, wave speed and range of patchy connections, so as to permit precise comparison with bar speeds, bar length, and OP difference in experimental data. On the other hand, the corresponding experimental data currently available in the literature is incomplete with respect to all possible bar angles and bar speeds, so improved experimental data would also facilitate comparison. For psychophysical data, improved estimates of bar speed (as projected to cortical level) and wave speed would confirm whether or not the model correctly predicts the appearance of motion streaks, and visual jittering, at the correct ratios of bar speed wave speed at various bar angles and lengths.

Conventional anatomical tests are possible in regard to the terminations of patchy connections in the periphery of the patch-free areas about singularities. As indicated in Figure 4, two populations of synaptic connections should be demonstrable in principle, by double injection/staining methods, near the singularity/patch edge.

As exemplified in Figure 5, observation of LFPs during the passage of a stimulating bar should reveal patterns of cRF activation with similar characteristics. The animations of the simulations also provide material for comparison in experiments outside that of single macrocolumns. Figure 9 gives an instance. This frame from a simulation shows a line moving from left to right, oriented orthogonally

For Peer Review

to the direction of motion, travelling with bar speed/wave speed = 0.8. The black arrow of the central macrocolumn indicates an OP response that is intermediate between those of the OP responses in the top and bottom macrocolumns – which themselves indicate orthogonal OP responses. Comparison with Figure 5 shows that at low bar speeds, disparities between adjacent macrocolumns are not predicted.

[Figure 9 about here]

No confirmation exists of Möbius-like patterns of connections in cortex, but Markram and colleagues (Perin et al 2011) found that pyramidal neuron networks cluster into multiple groups of a few dozen neurons each, with the neurons composing each group typically more than 100 μm apart, allowing for multiple groups to be interlaced in the same space. Connections between groups were relatively sparse, and of necessity linkages between interlaced groups were not exhaustively mapped, so interlinkages between groups to form Möbius-like networks, while possible, are neither proven nor disproven (see Figure 10). Further work using similar methods might support or disprove this inference. However, anatomical demonstration by this means may be is subject to a major difficulty – the temporal plasticity of synaptic connections near singularities (Dragoi et al 2001) – which may mean that the two conditions shown in Figure 10 are capable of alternation and reassembly in many detailed variants. A related caveat is that the Möbius organization may be clear-cut only in the late antenatal and pre-experiential stage of development, and might be wholly or partially overwritten by later developments during visual experience, as further considered in the Discussion.

[Figure 10 about here]

Discussion

To recap, in line with assumptions made in our earlier model (Wright et al 2006; Wright & Bourke 2008) we have assumed that (a) the equilibrium state of the activated cortex is zero-lag synchronous oscillation (b) Hebbian learning at synapses is modulated by pre-synaptic cooperative effects from nearby synapses (c) synaptic competition for metabolic resources permits only about a half of synapses to develop to a saturated state - and have added the further assumption that (d), in early cortical development lateral connections are isotropic, and decline exponentially with distance on two scales . The further assumption yielded a model now including the superficial patch system, and a

For Peer Review

rationale for the detailed simulation of signal transmission across the cortex. More detailed understanding of the processes and priorities underlying early cortical development might make the *a priori* assumption of two scales of connection unnecessary, as two scales of connection may emerge under the aegis of maximized stability and information transfer, as suggested by the *in vivo* neuron growth experiments of Nasuto and colleagues (Downes et al 2012).

We have accounted for the hexagonal periodicity of OP and the patch system in some species (Paik and Ringarch 2011) and the absence of any such clear organization in others (Horton and Adams 2005). Muir and colleagues (Muir et al 2011) commenting on interspecies difference in the orderliness of superficial patchy connections, remark that the differences between rodents, which lack both smooth OP organization and a superficial patch system, and primates and felines, which have well organized systems of both types, cannot lie in the species' lines of inheritance, since rodents are more closely related to primates than primates are to cats. They suggest that, alternatively, the difference may lie in one or more developmental parameters – for example the smaller size of visual cortex, or the degree of like-to-like preference exhibited by the superficial layer neurons. Our findings are consistent with both these possibilities. The emergence of a strongly hexagonal patch configuration came from the parameter choices $\lambda_\alpha << \lambda_\beta$ and $N_\beta >> N_\alpha$. These constraints imply longer-range signal transmission, and the possibility of more focal terminal distribution of the fibres in the patch system.

We have also found in the self-organization of α and β-patches a mechanism via which information transfer within the cortical field may lead to the absence of patchy connections about the singularities, in answer to the problem posed by Muir and Douglas (Muir and Douglas 2011). Our model is consistent with further findings from that group (Muir et al 2011) who have shown that "the patch system and cortical responses display a well-defined signature of their spatial configuration…this configuration is shared between the anatomical and functional systems [and] …the clustered projections…promote the expression of cortical activity states that correspond to statistical expectations of regularity in the visual world". Our model defines this description in terms of lag transmission of activity in the surrounding cortex to the areas surrounding each singularity.

As a critical test, we have shown that the Möbius model is able to explain increasing variation of apparent OP for increasingly rapid moving lines at variable angles of attack (Basole et al 2003) and in doing so does not depend on the assumption of fixed feature-detection attributes of particular cells whereas standard models – all those based upon alignment of excitatory connections and "like to like"

For Peer Review

couplings - are unable account for the same experimental data. The only other available explanation for the same data is to suppose individual V1 cells have intrinsic responses to spatial and temporal Fourier components in cortical signals (Baker and Issa 2005; Mante and Carandini 2005). This alternative is equivalent to the Möbius model in the sense that Fourier and time-series analyses are equivalent, but we have shown that assumption of individual cell tuning to particular frequency bands is not required. Since the our model depends upon wave transmission over patchy connections, it is also in accord with observations of traveling and standing waves in V1 associated with stimulus responses (Benucci et al 2007).

There is a further concordance of all these ideas with the findings of Dragoi and colleagues (Dragoi et al 2001) who showed "the existence of a map of orientation plasticity, closely related to the map of orientation preference, in which pinwheel centers constitute foci of plasticity and the orientation gradient is a measure of the degree of plasticity across V1." That is, they found plasticity of responses near OP singularities, and lack of plasticity in linear zones – the areas of strong patchy connection termination. This is to be expected if the patch system is composed of well consolidated connections suitable for consistent transmission with delay from fixed points in V1, while of the other hand, more complex, continually modified, information processing goes on in the areas around singularities. Since the local map is a folded representation of the space around each macrocolumn, the Möbius configuration would facilitate the expression of transient cross-correlations in signal inputs, since the folded structure minimizes average distances of separation between points on the local map. Transient short-range couplings, subject to rapid modulation in response to synaptic metabolic competition, created and decaying in response to inputs received via patchy connections, would permit the system to exploit the information representation capacity implicit in the model. We have assumed that synapses exhibit maximum Shannon entropy based on unconditional probabilities, whereas their mutual information would specify a specific pattern of information flow. The Möbius configuration may be a ground state of the synaptic configuration, the mutual information of the synaptic connections representing the average cross-correlation structure of stimulus space in the absence of structured inputs, but providing a base structure for transient representations. For the case of long-range, line-like visual stimuli, the transient representations would occur as local breakdowns of the Möbius structure, tending toward a structure similar to the standard models, although arising by a different mechanism, and in that case, such transient fluctuations in connectivity can be given a shorthand representation:

$$\mathbf{r}^2 \leftrightarrow \mathbf{r}^{[2]} \qquad (11)$$

For Peer Review

The antenatal development of response maps (Wiesel and Hubel 1974; Blakemore and Van Sluyters 1975; Sherk and Stryker 1976) presents no paradox, since emergence of the Möbius configuration does not depend upon structured visual stimuli. EEG activity progressively matures toward alternating synchronous and asynchronous states in the later antenatal period (Marks et al 1995; Mirmiran 1995) providing the co-ordination of pre-synaptic activity required for initial synaptic self-organization. With post-natal development and learning, the Möbius pattern may, as argued above, become to some extent, permanently or transiently overlain with connections storing specific correlations characteristic of the stimulus field, superimposed on the pre-experiential framework. This supposition implies that anatomical tests of the model might be better conducted on the pre-experiential cortex, since a flexible capacity for temporary or permanent overwriting of the Möbius configuration would increase the difficulties of anatomical testing.

If this model is confirmed by subsequent anatomical evidence there are wide implications for cortical information processing. Cortical dynamics could then be considered in terms of two interacting global attractors – an attractor for pulses (the equilibrium synchronous field) and an attractor for synaptic configuration (the patch-connected Möbius networks). To the writers' knowledge, no detailed dynamical theory along those lines has been developed. On the other hand, the proposed synaptic organization is an old friend in disguise - each macrocolumn an homologous map of surrounding cortex, in a form concealed by the folding of synaptic networks. The smaller scale of contextual connections is thus similar to the homologous spatial organization of primary sensory and motor cortices and elsewhere in the brain (Kaas 1997) – so each macrocolumn does not primarily receive information about concurrent correlated features, but instead gathers spatially distributed information from its neighbors, with temporal context determined by conduction delays. This suggests that cortical information transfer may depend upon superposition of spatio-temporal images at multiple scales and levels of cortical organization however modified these images become during later learning.

Appendix

……..

Derivation of pre-/post-synaptic pulse coincidence rates, $C_{\mathbf{R}}^{\mathbf{q}}$ and $C_{\mathbf{r}}^{\mathbf{q}}$

A general form of neural field equations (Wright 2009, 2010) is

$$\varphi_q(\mathbf{r},t) = \int f_q(\mathbf{r},\mathbf{r}')Q_q(\mathbf{r}',t-\frac{|\mathbf{r}-\mathbf{r}'|}{v})d\mathbf{r}' \qquad (1.1)$$

For Peer Review

$$V_q(\mathbf{r},t) = G(V_q(\mathbf{r}), \sum_{q=e \wedge q=i} \varphi_q(\mathbf{r}))(t-\tau) * f_s(\tau)) \quad (1.2)$$

$$Q_q(\mathbf{r},t) = f_\Sigma(V_q(\mathbf{r},t)) \quad (1.3)$$

where $\varphi; Q; V$, are afferent synaptic flux, pulse density, and dendritic voltage (LFP).

Subscript $q = e,i$ refers to excitatory or inhibitory neurons; $\mathbf{r},\mathbf{r}'$ are cortical positions.

$f_q(\mathbf{r},\mathbf{r}')$ is density of afferent axo-synaptic couplings with axonal conduction velocity ν.

$G(t-\tau) * f_s(\tau)$ is the nonlinear transformation of the excitatory and inhibitory synaptic flux into dendritic potentials.

$f_\Sigma(V_q(\mathbf{r},t))$ describes the local conversion of dendritic potentials into action potentials.

With parameters set to physiological values, equilibrium solutions are oscillating zero-lag synchronous fields regulated in amplitude by cortical activation. For small deviations of pulse rates from their mean values, equations (1.1-1.3) can be represented with regard to the excitatory cells alone, as

$$Q(\mathbf{q},t) = \int f(\mathbf{q},\mathbf{R}) Q(\mathbf{R}, t - \frac{|\mathbf{q}-\mathbf{R}|}{\nu}) d(\mathbf{q}-\mathbf{R}) + Q_{noise}(\mathbf{q},t) \quad (1.4)$$

$$\int f(\mathbf{q},\mathbf{R}) d(\mathbf{q}-\mathbf{R}) = \int f_\alpha(\mathbf{q},\mathbf{R}) d(\mathbf{q}-\mathbf{R}) + \int f_\beta(\mathbf{q},\mathbf{r}) d(\mathbf{q}-\mathbf{r}) = 1 \quad (1.5)$$

$$f_\alpha(\mathbf{q},\mathbf{R}) = \frac{N_\alpha}{N} \alpha \frac{1}{\lambda_\alpha} \exp[-\lambda_\alpha |\mathbf{q}-\mathbf{R}|] \quad (1.6)$$

$$f_\beta(\mathbf{q},\mathbf{r}) = \frac{N_\beta}{N} \beta \frac{1}{\lambda_\beta} \exp[-\lambda_\beta |\mathbf{q}-\mathbf{r}|] \quad (1.7)$$

$\mathbf{r}$ and $\mathbf{R}$ are vector positions distant from $\mathbf{q}$, measured along short-range and longer-range connections respectively.

Q excitatory point pulse-emission rate.

Q_{noise} Poisson-distributed spike trains – in the activated state, of small amplitude relative to amplitude of oscillation .

ν axonal conduction speed.

For Peer Review

f_α distribution of long range axonal tree synaptic density.

f_β distribution for short range (intracortical) axonal tree synaptic density.

N number of excitatory synapses per neuron.

N_α, N_β number of synapses per neuron from long range and short range respectively, $N_\beta > N_\alpha$.

$\lambda_\alpha, \lambda_\beta$ inverse length constants for synaptic density, $\lambda_\alpha << \lambda_\beta$.

$\alpha, \beta = 1$ ground value of synaptic gain.

The field is stabilized by inhibitory feedbacks, which generate a zero-lag synchronous oscillation. In the presence of superadded noise the fraction of pre-synaptic pulses, from cells at some other given position, and post-synaptic pulses at the reference point $\mathbf{q}$, that coincide, is given by $r \in \{0-1\}$ - a function which declines with the distance of separation. The mean field excitatory pulse rate $\overline{Q}$, and the mean value of r, is regulated by cortical activation.

Therefore pre-/post-synaptic pulse coincidence rates, $C^{\mathbf{q}}_{\mathbf{R}}$ and $C^{\mathbf{q}}_{\mathbf{r}}$, can be defined as

$$C^{\mathbf{q}}_{\mathbf{r},\mathbf{R}} = [coincident\ fraction\ of\ pre-\&\ post-synaptic\ pulses] \times [mean\ pre-synaptic\ pulse\ density] \times [mean\ post-synaptic\ pulse\ rate]$$

and thus

$$C^{\mathbf{q}}_{\mathbf{R}} = r\frac{N_\alpha}{N}\frac{1}{\lambda_\alpha}\exp[-\lambda_\alpha|\mathbf{q}-\mathbf{R}|]\overline{Q}^2 \qquad (1.8)$$

$$C^{\mathbf{q}}_{\mathbf{r}} = r\frac{N_\beta}{N}\frac{1}{\lambda_\beta}\exp[-\lambda_\beta|\mathbf{q}-\mathbf{r}|]\overline{Q}^2 \qquad (1.9)$$

……..

Funding

This work was supported by the Frank P. Hixon Fund of the California Institute of Technology and the Oakley Foundation of New Zealand in grants to JJW - and by iVEC, through the use of advanced computing resources located at the University of Western Australia by PDB.

Acknowledgements

For Peer Review

Special thanks are due to Adrienne Wright.

Conflict of Interest: none declared.

References

Albert MV, Schnabel A, Field DJ. 2008. Innate visual learning through spontaneous activity patterns. PLoS Computational Biology. 10.1371/journal.pcbi.1000137

Alexander DM, Bourke PD, Sheridan P, Konstandatos O, Wright JJ. 2004. Intrinsic connections in tree shrew V1 imply a global to local mapping. Vision Research, 44: 857–876.

Angelucci A, Levitt JB, Lund JS. 2002.Anatomical origins of the classic receptive field and modulatory surround field of single neurons in macaque visual cortical area V1. Prog. Brain. Res. 136: 373-388.

Baker TI, Issa NP. 2005. Cortical maps of separable tuning properties predict population responses of complex visual stimuli. J. Neurophysiol. 94: 775-787.

Basole A, White LE, Fitzpatrick D. 2003. Mapping of multiple features in the population response of visual cortex. Nature. 423: 986-990.

Basole A, Kreft-Kerekes V, White LE, Fitzpatrick D. 2006. Cortical cartography revisited: a frequency perspective on the functional architecture of visual cortex. Progress in Brain Research. 154: DOI: 10.1016/S0079-6123(06)54006-3.

Benucci A, Frazor RA, Carandini M. 2007. Standing waves and traveling waves distinguish two circuits in visual cortex. Neuron. 55: 103-117.

Blakemore C, Van Sluyters RC. 1975. Innate and environmental factors in the development of the kitten's visual cortex. J. Physiol. (Lond.). 248: 663-716.

Boucsein C, Nawrot M, Schnepel P, Aertsen A. 2011. Beyond the cortical column: abundance and physiology of horizontal connections imply a strong role for inputs from the surround. Frontiers of Neuroscience. 5: doi: 10.3389/fnins.2011.00032.

For Peer Review

Buzás P, Kovács K, Ferecskó AS, Budd JML, Eysel UT, Kisvárday ZF. 2006. Model-based analysis of excitatory lateral connections in the visual cortex. J. Comp. Neurol. 499: 861-881.

Bressler, SL, Coppola R, Nakamura R. 1993. Episodic multiregional cortical coherence at multiple frequencies during visual task performance. Nature. 366: 153–156.

Bringuier V, Chavane F, Glaeser L, Frégnac Y. 1999. Horizontal propagation of visual activity in the synaptic integration field of area 17 neurons. Science 283: 695-699.

Callaway EM, Katz LC. 1990. Emergence and refinement of clustered horizontal connections in cat striate cortex. J. Neurosci. 10: 1134-1153.

Carpenter GA, Grossberg S, Rosen DB. 1991. Fuzzy ART: fast stable learning and categorization of analog patterns by an adaptive resonance system. Neural Networks. 4: 759-771.

Carriera-Perpiñán MÁ, Lister RJ, Goodhill GJ. 2005. A computational model for development of multiple maps in primary visual cortex. Cerebral Cortex. 15: 1222-1233.

Chapman CL, Bourke PD, Wright JJ. 2002. Spatial eigenmodes and synchronous oscillation: coincidence detection in simulated cerebral cortex. J. Math. Biol. 45: 57-78.

Cohen MR, Kohn A. 2011. Measuring and interpreting neuronal correlations. Nature Neuroscience. 14: 811-819.

DeAngelis GC, Ohzawa I, Freeman RD. 1993. Spatiotemporal organization of simple-cell receptive fields in the cat's striate cortex. I. General characteristics and postnatal development. J Neurophysiol. 69: 1091–1117.

Downes JH, Hammond MW, Xydas D, Spencer M, Becerra VM, Warwick K, Whalley BJ, Nasuto SJ. (2012) Emergence of a small-world functional network in cultured neurons. PLoS Computational Biology. (in press)

Dragoi V, Rivadulla C, Sur M. 2001. Foci of orientation plasticity in visual cortex. Nature 411: 80-86.

Durbin R, Mitchison G. 1990. A dimension reduction framework for understanding cortical maps. Nature. 343: 644-647.

Durack JC, Katz LC. 1996. Development of horizontal projections in layer 2/3 of ferret visual cortex. Cerebral Cortex. 6: 178-183.

For Peer Review

Durbin R, Willshaw DJ. 1987. An analogue approach to the travelling salesman problem using an elastic net method. Nature. 326: 689-691.

Eckhorn R, Bauer R, Jordon W, Brosch M, Kruse W, Monk M. Reitboeck HJ. 1988. Coherent oscillations: a mechanism of feature linking in the in the visual cortex? Biol. Cybern. 60: 121–130.

Eckhorn R, Reitboeck HJ, Arndt M, Dicke P. 1990. Feature linking via synchronization among distributed assemblies: simulations of results from cat visual cortex. Neural Computation. 2: 293-307.

Elliott T, Shadbolt NR. 2002. Multiplicative synaptic normalization and a nonlinear Hebb rule underlie a neurotrophic model of competitive synaptic plasticity. Neural Computation. 14: 1311-1322.

Elliot T. 2011. Stability against fluctuations: scaling, bifurcations, and spontaneous symmetry breaking in stochastic models of synaptic plasticity. Neural Computation. 23: 674-734.

Enoki R, Hu Y-L, Hamilton D, Fine A. 2009. Expression of long-term plasticity at individual synapses in hippocampus is graded, bi-directional, and mainly pre-synaptic: optic quantal analysis. Neuron. 62: 242-253.

Freeman WJ. 1975. Mass Action in the Nervous System. New York: Academic Press. In: Induced rhythms of the brain. Boston: Berkhäuser.

Freeman WJ. 1991. Predictions on neocortical dynamics derived from studies in paleocortex.

Gilbert CD and Wiesel TN. 1979. Morphology and intracortical projections of functionally characteristic neurons in cat visual cortex. Nature. 280: 120-125.

Gilbert CD and Wiesel TN. 1989. Columnar specificity of intrinsic horizontal and corticocortical connections in cat visual cortex. J. Neurosci. 9: 2432-2442.

Gray CM, Konig P, Engel AK, Singer W. 1989. Oscillatory responses in cat visual cortex exhibit intercolumnar synchronisation which reflects global stimulus properties. Nature. 388: 334–337.

Grossberg S, Olson SJ. 1994. Rules for the cortical map of ocular dominance and orientation columns. Neural Networks. 7: 883-894.

Haken, H. 1976. Principles of brain functioning. Berlin: Springer.

For Peer Review

Hassenstaub A, Shu Y, Haider B, Krauschaar U, Duque A, McCormick DA. 2005. Inhibitory postsynaptic potentials carry synchronized frequency information in active cortical networks. Neuron. 47: 423-435.

Harris AE, Ermentrout GB, Small SL. 1997. A model of ocular column development by competition for trophic factor. Proc. Natl. Acad. Sci. USA. 94: 9944-9949.

Hirsch JA, Gilbert CD. 1991. Synaptic physiology of horizontal connections in the cat's visual cortex. J. Neurosci. 11: 1800-1809.

Horton CH, Adams DL. 2005. The cortical column: a structure without a function. Phil. Trans. R. Soc. B. 360: 837-862.

Hubel DH, Wiesel TN. 1959. Receptive fields of single neurones in the cat's striate cortex. Journal of Physiology. 148: 574-591.

Jirsa, VK, Haken, H. 1996. Field theory of electromagnetic brain activity. Phys. Rev. Lett., 77: 960–963.

Kaas JH. 1997. Topographical maps are fundamental to sensory processing. Brain Research Bulletin. 44: 107-112.

Kohonen T. 1982. Self-organized formation of topologically correct feature maps. Biol. Cybern. 43: 59-69.

Kveraga K, Ghuman AS, Bar M. 2007. Top-down predictions in the cognitive brain. Brain and Cognition 65: 145-168.

Linsker R. 1986a. From basic network principles to neural architecture: emergence of spatial-opponent cells. Proc. Natl. Acad. Sci. USA 83: 7508-7512.

Linsker R. 1986b. From basic network principles to neural architecture: emergence of orientation selective cells. Proc. Natl. Acad. Sci. USA 83: 8390-8394.

Linsker R. 1986c. From basic network principles to neural architecture: emergence of orientation columns. Proc. Natl. Acad. Sci. USA 83: 8779-8783.

McGuire BA, Gilbert CD, Rivlin PK, Wiesel TN. 1991. Targets of horizontal connections in macaque primary visual cortex. J. Comp. Neurol. 305: 370-392.

For Peer Review

Mariño J, Schummers J, Lyon DC, Schwabe L, Beck O, Wiesing P, Obermayer K, Sur M. 2005. Invariant computations in local cortical networks with balanced excitation and inhibition. Nat. Neurosci. 8: 194-201.

Marks GA, Shaffery JP, Okensberg A, Speciale SG, Roffwarg HP. 1995. A functional role for REM sleep in brain maturation. Behavioural Brain Research 69: 1-11.

Malsberg, von der C. 1973. Self organization of orientation sensitive cells in the striate cortex. Kybernetic. 14: 85-100.

Mante V, Carandini M. 2005. Mapping of stimulus energy in primary visual cortex. J. Neurophysiol. 94: 788-798.

Merigan WH, Maunsell JHR. 1993. How parallel are the primate visual pathways? Annu. Rev. Neurosci. 16: 369-402.

Miller KD. 1994. A model for the development of simple cell receptive fields and the ordered arrangement of orientation columns through the activity dependent competition between ON- and OFF-center inputs. J. Neurosci. 14: 409-441.

Mirmiran M. 1995. The function of fetal/neonatal rapid eye movement sleep. Behavioural Brain Research. 69: 13-22.

Mitchison G, Crick F. 1982. Long axons within the striate cortex: distribution, orientation and patterns of connections. Proc. Natl. Acad. Sci. USA. 79: 3661-3665.

Muir DR, Douglas RJ. 2011. From neural arbours to daisies. Cerebral Cortex. 21: 1118-1133.

Muir DR, Da Costa NMA, Girardin CC, Naaman S, Omer DB, Ruesch E, Grinvald A, Douglas RJ. Embedding of cortical representations by the superficial patch system. Cerebral Cortex. 21: 2244-2260.

Miyashita M, Tanaka S. 1992. A mathematical model for the self-organization of orientation columns in visual cortex. NeuroReport. 3: 69-72.

Nunez, P. L. 1981. Electric fields of the brain. London: Oxford University Press.

O'Connor DH, Wittenberg GM, Wang SS-H. 2005a. Dissection of bidirectional synaptic plasticity into saturable unidirectional processes. J. Neurophysiol. 94: 1565-1573.

For Peer Review

O'Connor DH, Wittenberg GM, Wang SS-H. 2005b. Graded bidirectional synaptic plasticity is composed of switch-like unitary events. Proc. Natl. Acad. Sci. USA. 102: 9679-9684.

Obermayer K, Ritter H, Schulten K. 1990. A principle for the formation of the spatial structure of cortical feature maps. Proc. Natl. Acad, Sci. USA 87: 8345-8349.

Obermayer K, Ritter H, Schulten K. 1992. A model for the development of the spatial structure of retinotopic maps and orientation columns. IEICE Trans. Fundamentals. E75A: 537-545.

van Ooyen A, Willshaw DJ. 1999. Competition for neurotrophic factor in the development of nerve connections. Proc. R. Soc. Lond. B. 266: 883-892.

van Ooyen A. 2001. Competition in the development of nerve connections: a review of models. Network: Comput. Neural Syst. 12: R1-R47.

Paik S-B, Ringach DL. 2011. Retinal origin of orientation maps in visual cortex. Nature Neuroscience 14: 919-925.

Perin R, Berger TK, Markram H. 2011. A synaptic organizing principle for cortical neuronal groups. PNAS. 108: 5419-5424.

Price DJ. 1986. The postnatal development of clustered intrinsic connections in area 18 of the visual cortex in kittens. Dev. Brain Res. 24: 31-38.

Rao RPN, Ballard DH. 1997. Dynamic model of visual recognition predicts neural response properties in the visual cortex. Neural Computation. 9:721-763.

Rennie CJ, Wright JJ, Robinson PA. 2000. Mechanisms of cortical electrical activity and the emergence of gamma rhythm. J. Theoret. Biol 205: 17–35.

Ringarch DL. 2007. On the origin of the functional architecture of the cortex. PLoS ONE. Issue 2 e251.

Robinson PA, Rennie CJ, Wright JJ. 1997. Propagation and stability of waves of electrical activity in the cerebral cortex. Phys. Rev. E. 56: 826–840.

Robinson PA, Rennie CJ, Wright JJ. 1998. Synchronous oscillations in the cerebral cortex. Physical Review E. 57: 4578–4588.

For Peer Review

Robinson PA, Rennie CJ, Wright JJ, Bahramali H, Gordon E, Rowe DL. 2001. Prediction of electroencephalographic spectra from neurophysiology. Phys Rev E 63: 701–702.

Rockland KS, Lund JS. 1983. Intrinsic laminar lattice connections in primate visual cortex. J. Comp. Neurol. 216: 303-318.

van Rotterdam A, Lopes da Silva FH, van den Ende J, Viergever MA, Hermans AJ. 1982. A model of the spatio-temporal characteristics of the alpha rhythm. Bull. Math Biol 44: 283–305.

Ruthazer ES, Stryker MP. 1996. The role of activity in the development of long-range horizontal connections in area 17 of the ferret. J. Neurosci. 16: 7253-7269.

Schillen TB, Konig P. 1994. Binding by temporal structure in multiple feature domains of an oscillatory neural network. Biol. Cybern. 70: 397–405.

Sharma J, Angelucci A, Rao SC, Sur M. 1995. Relationship of intrinsic connections to orientation maps in ferret primary visual cortex: iso-orientation domains and singularities. Presented at Society for Neuroscience, San Diego, CA.

Sherk H, Stryker MP. 1976. Quantitative study of orientation selectivity in visually inexperienced kittens. J. Neurophysiol. 39: 63-70.

Singer W.1999. Neuronal synchrony: a versatile code for the definition of relations? Neuron. 24: 49-65.

Steriade M. 2000. Corticothalamic resonance, states of vigilance and mentation. Neuroscience. 101: 243-276.

Swindale NV. 1982. A model for the formation of orientation columns. Proc. R. Soc. B. 215: 211-230.

Swindale NV. 1992. A model for the coordinated development of columnar systems in primate striate cortex. Biol. Cybern. 66: 217-230.

Swindale NV. 1996. The development of topography in the visual cortex: a review of models. Network: Computation in Neural Systems. 7: 161-247.

For Peer Review

Swindale NV. 2008. Feedback decoding of spatially structured population activity in cortical maps. Neural Computation. 20: 176-204.

Tanaka S. 1990. Theory of self-organization of cortical maps: mathematical framework. Neural Networks. 3: 625-640.

Traub RD, Whittington MA, Stanford IM, Jefferys JGR. 1996. A mechanism for generation of long-range synchronous fast oscillations in the cortex. Nature. 383: 621–624.

Tsukada M, Fukushima Y. 2010. A context dependent mechanism in hippocampal CA1 networks. Bull Math Biol. DOI 10.1007/s11538-010-9566-8.

Varshney LR, Sjöström PJ, Chklovskii DB. 2006. Optimal information storage in noisy synapses under resource constraints. Neuron. 52: 409-423.

Whittington MA, Faulkner HJ, Doheny HC, Traub RD. 2000. Neuronal fast oscillations as a target site for psychoactive drugs. Pharmacol. Ther. 86, 171–190.

Wiesel TN, Hubel DH. 1974. Ordered arrangement of orientation columns in monkeys lacking visual experience. J. Comp. Neurol. 158: 307-318.

Willshaw DJ, von der Malsberg C. 1976. How patterned neural connections can be be set up by self-organization. Proc. R. Soc. B. 194: 431-435.

Wilson HR, Cowan JD. 1973. A mathematical theory of the functional dynamics of cortical and thalamic nervous tissue. Kybernetik 13: 55–80.

Wright JJ, Bourke PD, Chapman CL. 2000. Synchronous oscillation in the cerebral cortex and object coherence: simulation of basic electrophysiological findings. Biol. Cybern. 83: 341-353.

Wright JJ, Rennie CJ, Lees GJ, Robinson PA, Bourke PD, Chapman CL, Gordon E, Rowe DL. 2003. Simulated electrocortical activity at microscopic, mesoscopic and global scales. Neuropsychopharmacology. 28: S80-S93.

Wright JJ, Alexander DM, Bourke PD. 2006. Contribution of lateral interactions in V1 to organization of response properties. Vision Research 46: 2703 – 2720.

Wright JJ, Bourke PD. 2008. An outline of functional self-organization in V1: synchrony,

For Peer Review

STLR and Hebb rules. Cognitive Neurodynamics 2: 147 – 157.

Wright JJ. 2009. Generation and control of cortical gamma: findings from simulation at two scales. Neural Networks. 22: 373-384.

Wright JJ. 2010. Attractor dynamics and thermodynamic analogies in the cerebral cortex: synchronous oscillation, the background EEG, and the regulation of attention. Bull. Math. Biol. DOI 10.1007/s1 1538-010-9562-z.

Yousef T, Tóth É, Rausch M, Eysel UT, Kisvárday ZF. 2001. Topography of orientation centre connections in the primary visual cortex of the cat. Neuroreport. 12: 1693-1699.

Legends for Figures

Figure 1.

Standard model.

Colours of the spectrum indicate OP.

Top: A cluster of seven macrocolumns in hexagonal configuration. OP for lines of orientation $0-\pi$ surround pinwheel singularities over angles $0-2\pi$, merging with neighbours to form linear zones and saddles. Lines of excitatory synaptic coupling of neurons, shown as transparent tubes, radiate about singularities, connecting "like to like" OP.

Bottom: inset from rectangle in diagram above, showing disposition of strengthened synaptic couplings (black) between mutually excitatory cells of unique OP, with synaptic couplings weakened by longer-range inhibition (white) surrounding the self-excitatory OP group.

Figure 2.

Patchy connections and singularities, self-organized in a synchronous neural field. Pale circles: neurons surrounding singularities, coupled by saturated short-range connections. Black circles: neurons giving rise to and receiving saturated long-range patchy connections. Grey background: neurons receiving saturated connections of both types. Dashed lines are of length

$$x = (\ln\frac{N_\beta \lambda_\alpha}{N_\alpha \lambda_\beta})/(\lambda_\beta - \lambda_\alpha).$$

Top: $N_\beta >>> N_\alpha$

For Peer Review

Bottom: $N_\alpha > N_\beta$

Figure 3.

Euclidean model.

Top: In the hexagonal configuration, OP for lines of orientation $0-\pi$ repeats twice about a singularity. Lines of excitatory synaptic coupling of neurons radiate about singularities. Patchy connections arise from cell bodies as in Figure 2 (Top), shown as large circled + and x signs. Their corresponding terminations on cells at the periphery of each macrocolumn are shown as small circled + and x signs.

Bottom: inset analogous to that in Figure 1, shows disposition of short-range saturated (black) and weaker (white) synaptic couplings.

Figure 4.

Möbius model.

Top: OP for lines of orientation $0-\pi$ surround singularities over $0-2\pi$. Lines of excitatory synaptic coupling of neurons are rolled into a meshwork that is closed over 4π. Patchy connections from opposite sides of the macrocolumn terminate on closely situated, but separate, cells, on the periphery of the singularities.

Bottom: inset shows short-range saturated (black) synaptic couplings are deployed along the Möbius mesh, and unsaturated (white) synaptic couplings bridge between opposite limbs of the mesh.

Figure 5.

Simulated signal transmission in the Möbius model. A line in the visual field (red line, here moving left to right, and orientated at 60 degrees to the line of passage)) is projected to a part of V1. Sequential frames, arranged top to bottom, show the beginning, middle and end of the time of activation (shown as illumination) of the cRFs of a row of macrocolunmns. Green lines are the red line's image, transferred via patchy connections to each macrocolumn, creating subthreshold activation. Black arrows show the angular averages of the green lines, to indicate the field in which cells respond maximally once triggered by the cRF. Bar length 6, Bar speed/wave speed = 0.5.

Figure 6.

Left side: OP difference versus bar speed/wave speed as a function of bar angle, for bar length of 4 units. Horizontal bars on plotted OP difference indicate SE.

For Peer Review

Right side: Insets show the central macrocolumn of the hexagonal group illustrated in Figure 5. Apparent OP (black arrow) is at the median time step of the averaging window, for bar angle 45 degrees, at high, intermediate and low bar speeds, with corresponding visual bar position (red), and area of subthreshold activation (green line and area of surrounding illumination).

Figure 7.

OP difference versus bar speed/wave speed as a function of bar angle, for bar lengths 0.25 unit (top), 1 unit (middle) and 16 units (bottom).

Figure 8.

Standard model. OP difference versus bar speed/wave speed as a function of bar angle, for the same bar length as in Figure 6, with angular overlap of excitation within the macrocolumn set to $\varphi = 45$ degrees.

Figure 9.

Predicted OP responses, ranging from -90 to $+90$ degrees, in adjacent macrocolumns in response to the transition of the center of a visual line, and the ends of the same line, at bar angle = zero degrees, and bar speed/wave speed = 0.8.

Figure 10.

Top: Pyramidal cell connections, on a scale equivalent to macrocolumns, form interwoven rings (red and blue lines) of connected cells, as demonstrated by Perin et al (2011). Dashed lines at 6 o'clock highlight closure of the rings over 2π and, at 11 o'clock, the occurrence of irregular bridging connections between rings.

Bottom: Hypothetical Möbius variant of the same structure. Dashed lines at 6 o'clock highlight closure of the rings over 4π and, at 11 o'clock, the occurrence of systematic bridging connections between rings, to maintain continuity of representation of positions.

For Peer Review

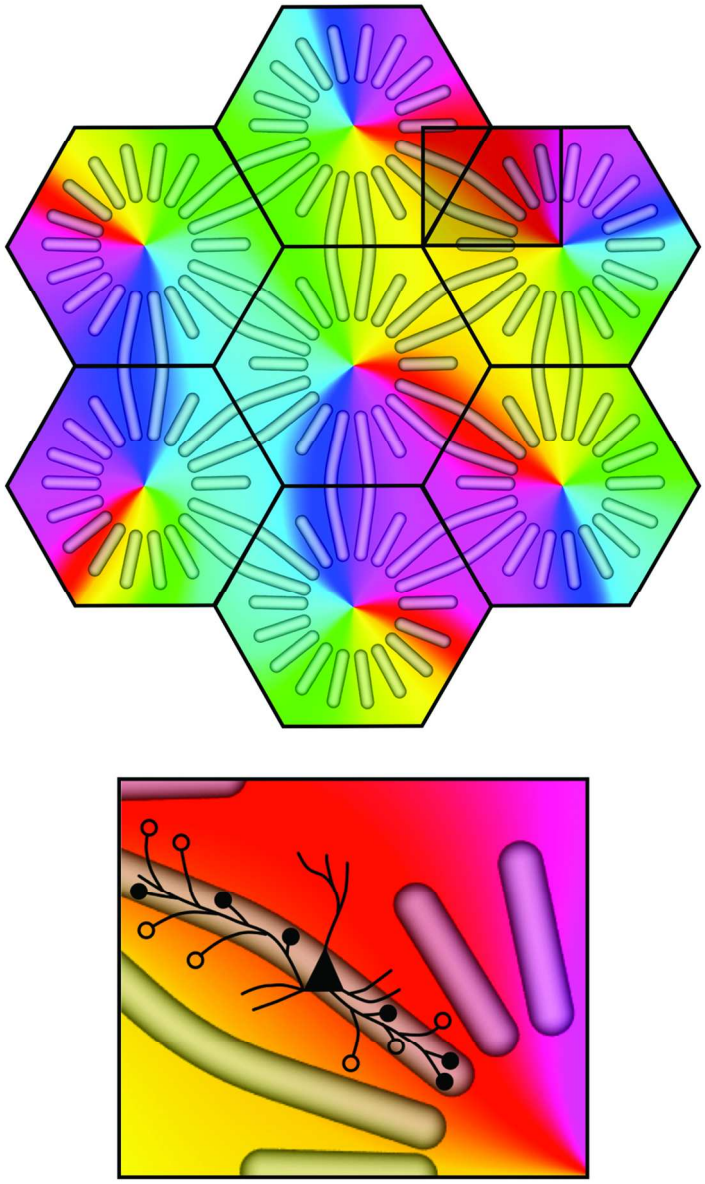

Figure 1
86x144mm (300 x 300 DPI)

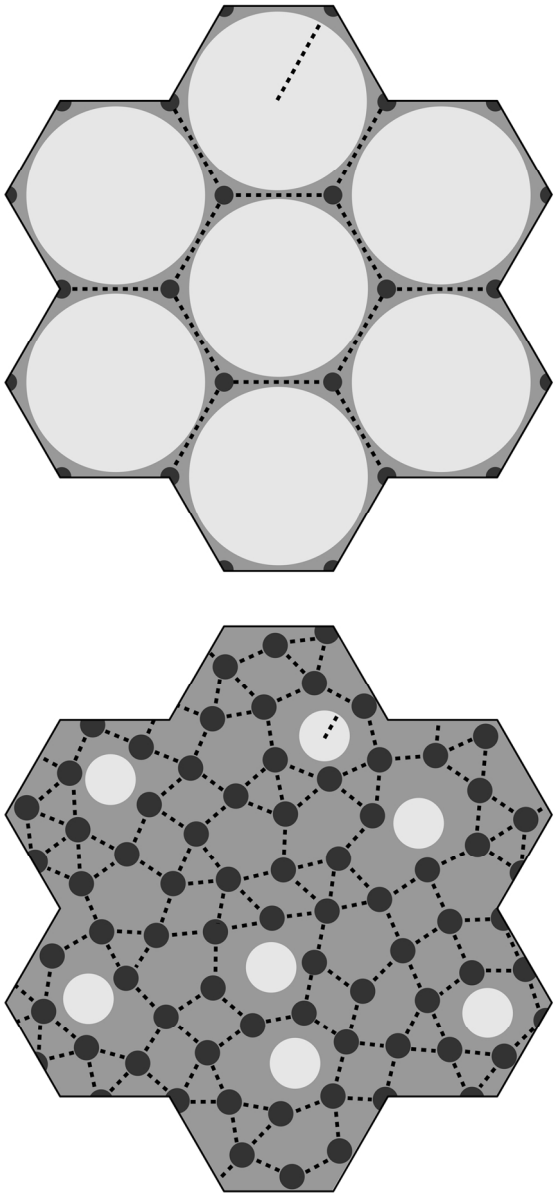

Figure 2
86x181mm (300 x 300 DPI)

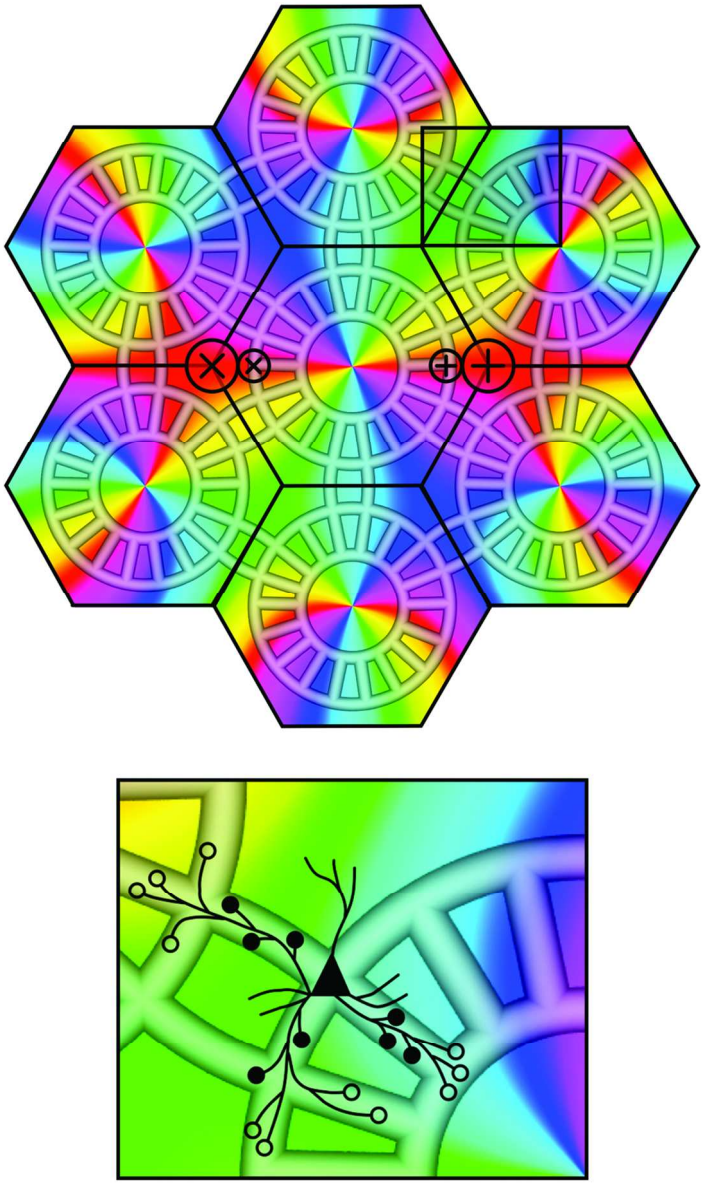

Figure 3
86x144mm (300 x 300 DPI)

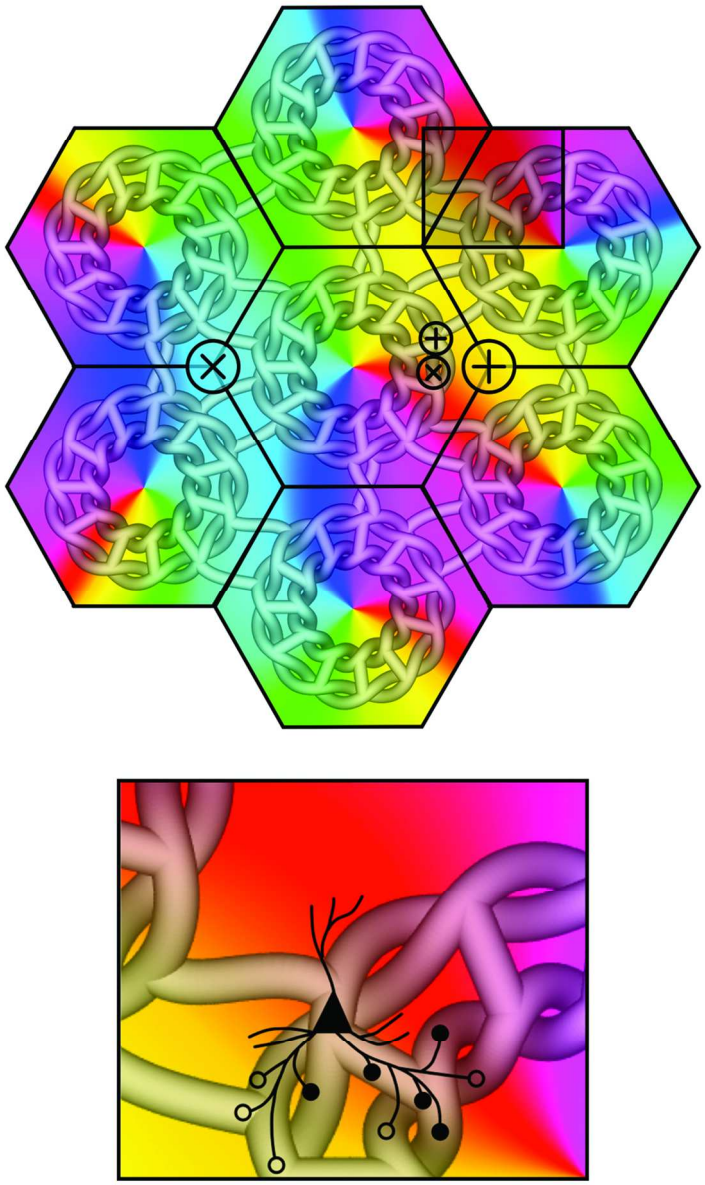

Figure 4
86x144mm (300 x 300 DPI)

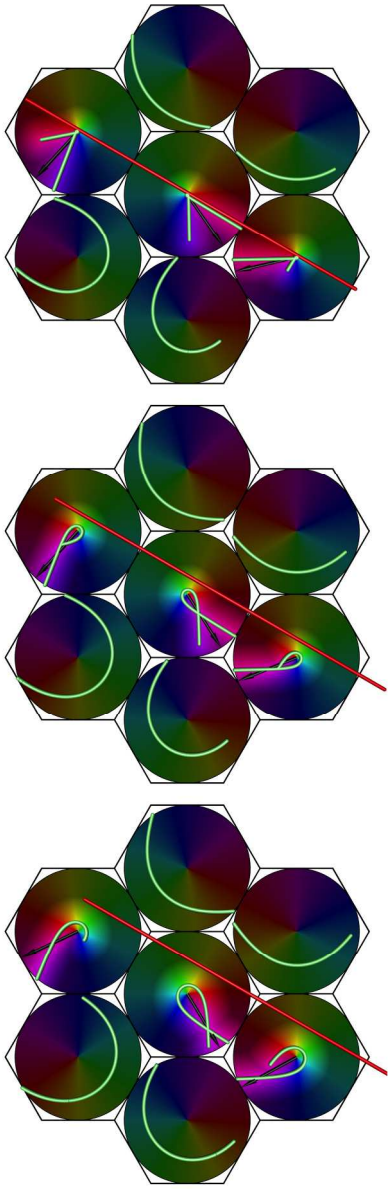

Figure 5
86x257mm (300 x 300 DPI)

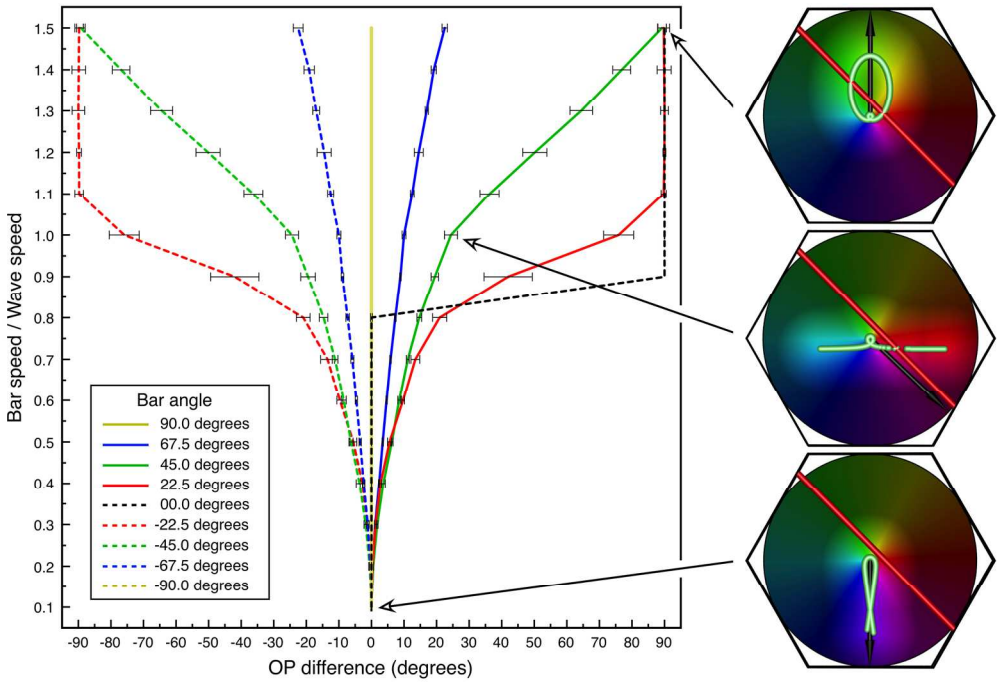

Figure 6
180x122mm (300 x 300 DPI)

Review

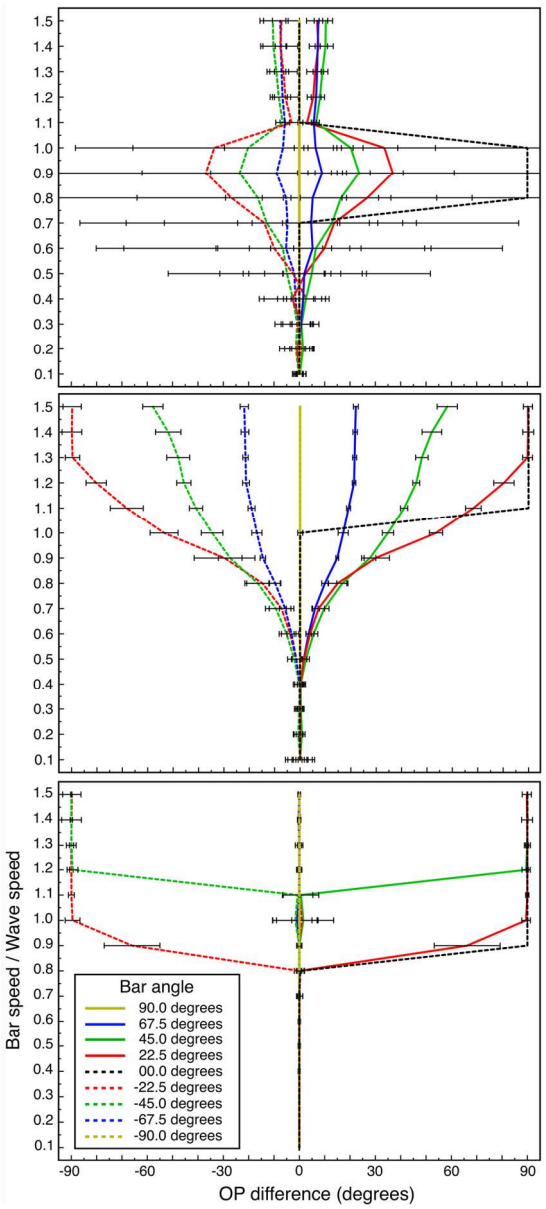

Figure 7
86x187mm (300 x 300 DPI)

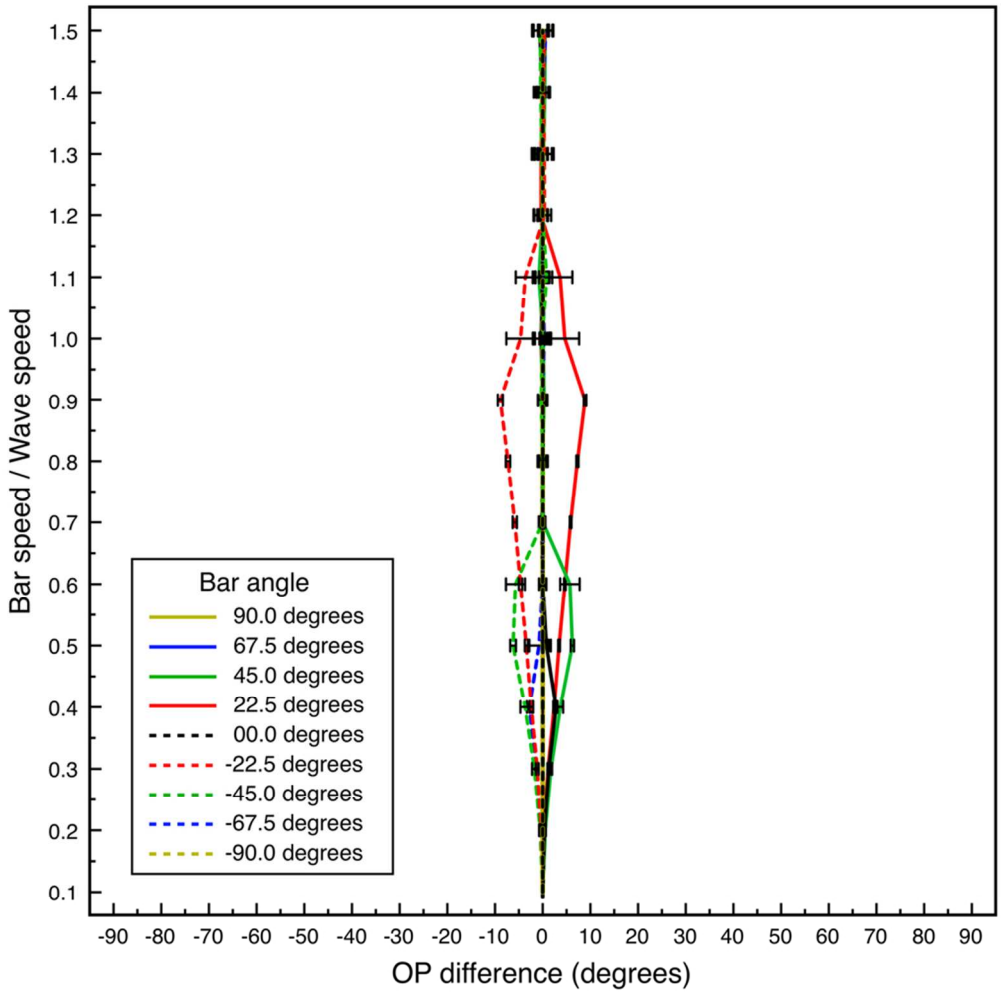

Figure 8
86x85mm (300 x 300 DPI)

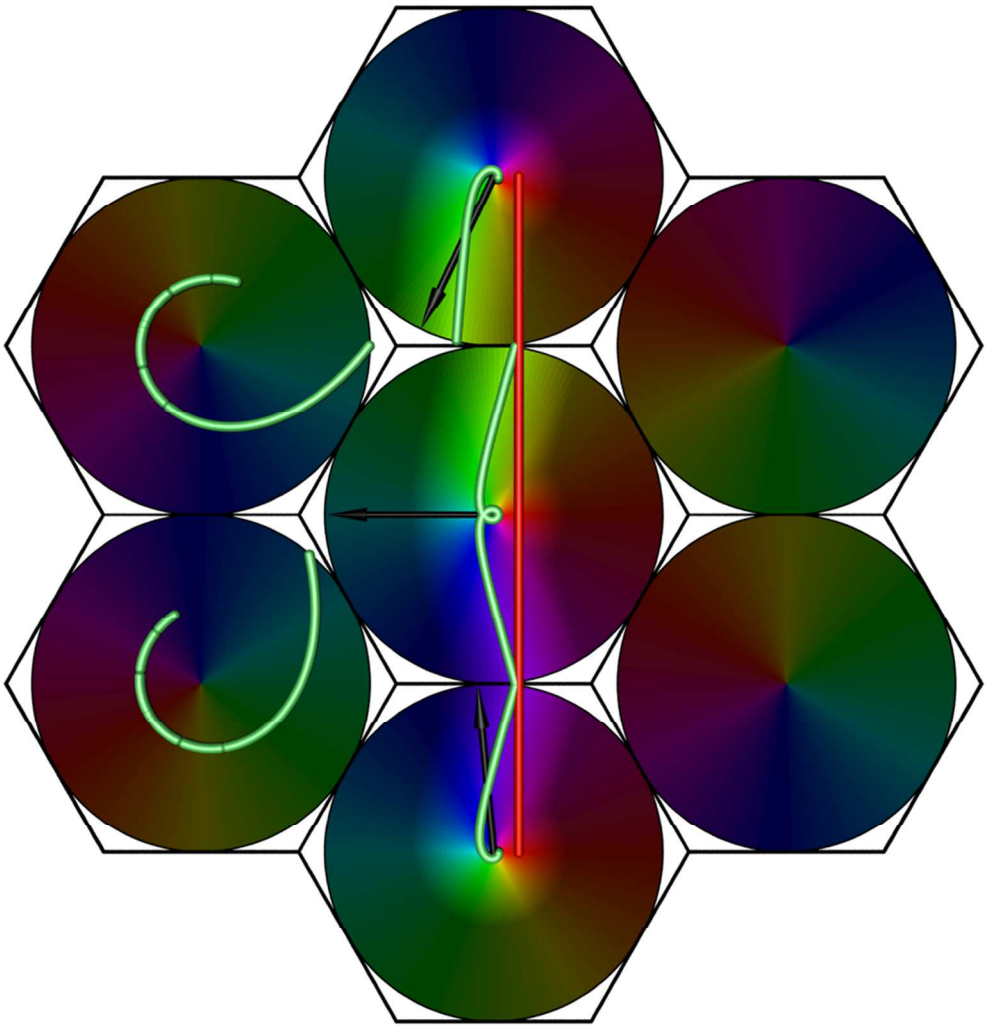

Figure 9
86x88mm (300 x 300 DPI)

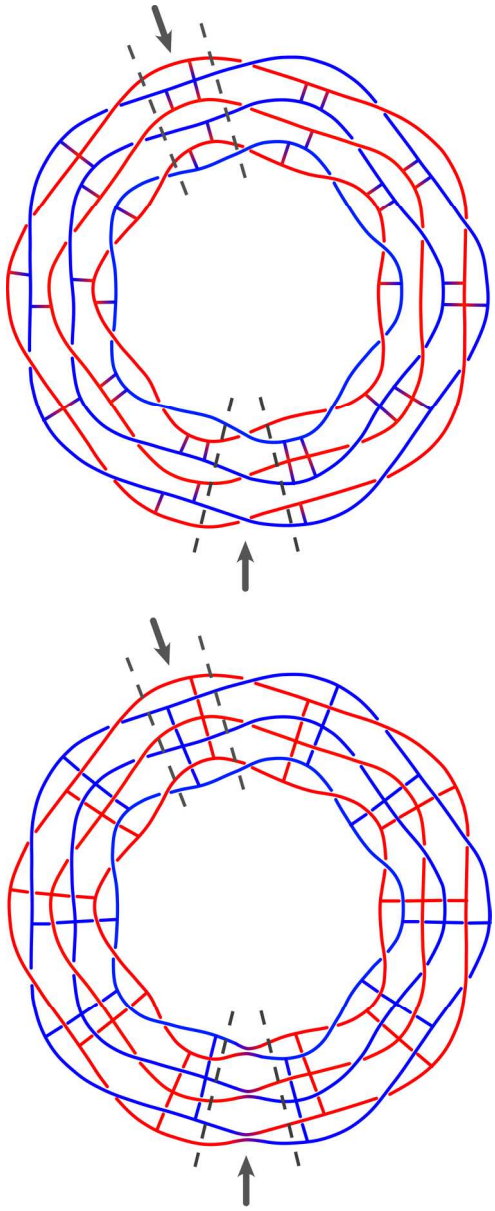

Figure 10
86x212mm (300 x 300 DPI)